AGU PUBLICATIONS

Geophysical Research Letters

RESEARCH LETTER
10.1002/2014GL061939

Key Points:
- We obtained density and dissipation measurements at the ocean surface
- We made estimates of the mixed (MLD) and mixing (XLD) layer depths
- We found a relationship between MLD and XLD for buoyancy-driven conditions

Correspondence to:
B. Ward,
bward@nuigalway.ie

Citation:
Sutherland, G., G. Reverdin, L. Marié, and B. Ward (2014), Mixed and mixing layer depths in the ocean surface boundary layer under conditions of diurnal stratification, *Geophys. Res. Lett.*, *41*, 8469–8476, doi:10.1002/2014GL061939.

Received 19 SEP 2014
Accepted 7 NOV 2014
Accepted article online 13 NOV 2014
Published online 4 DEC 2014

Mixed and mixing layer depths in the ocean surface boundary layer under conditions of diurnal stratification

G. Sutherland[1], G. Reverdin[2], L. Marié[3], and B. Ward[1]

[1]School of Physics, National University of Ireland, Galway, Ireland, [2]LOCEAN/Institut Pierre Simon Laplace, Expérimentation et Approches Numériques, Sorbonne Universités, (UPMC, Paris VI-Denis Diderot University), CNRS/IRD/MNHN, Université Pierre et Marie Curie Paris, France, [3]Laboratoire de Physique des Océans, UMR 6523 CNRS/IFREMER/IRD/UBO, Plouzané, France

Abstract A comparison between mixed (MLD) and mixing (XLD) layer depths is presented from the SubTRopical Atlantic Surface Salinity Experiment (STRASSE) cruise in the subtropical Atlantic. This study consists of 400 microstructure profiles during fairly calm and moderate conditions ($2 < U_{10} < 10$ m s^{-1}) and strong solar heating O(1000 W m^{-2}). The XLD is determined from a decrease in the turbulent dissipation rate to an assumed background level. Two different thresholds for the background dissipation level are tested, 10^{-8} and 10^{-9} m^2 s^{-3}, and these are compared with the MLD as calculated using a density threshold. The larger background threshold agrees with the MLD during restratification but only extends to half the MLD during nighttime convection, while the lesser threshold agrees well during convection but is deeper by a factor of 2 during restratification. Observations suggest the use of a larger density threshold to determine the MLD in a buoyancy driven regime.

1. Introduction

The ocean surface boundary layer (OSBL) is typically defined by a quasi-homogeneous density structure which can range from a few metres to several hundred meters in depth and is created by turbulent mixing forced by the wind, surface gravity waves, and convective cooling. This surface mixed layer is an important component of the global climate system as it controls the transfer of heat, momentum, and trace gases between the atmosphere and the ocean [*Belcher et al.*, 2012].

Definitions for the depth of the OSBL are usually based on the quasi-homogeneous density structure, i.e., the mixed layer depth (MLD, denoted by h_ρ). The use of a density threshold relative to a reference depth is the most common, which defines an acceptable density variability within the mixed layer usually in the range $\Delta\rho = 0.01$–0.03 kg m^{-3} [*Thomson and Fine*, 2003; *de Boyer Montégut et al.*, 2004]. There are many other definitions such as using a temperature threshold [*Kara et al.*, 2000], a density gradient threshold [*Lukas and Lindstrom*, 1991], a linear optimal fitting approach [*Chu and Fan*, 2011], a split-merge method based on the profile shape [*Thomson and Fine*, 2003] or dissolved oxygen profiles [*Castro-Morales and Kaiser*, 2012]. What all these processes have in common is that they are trying to characterize the dynamic boundary layer depth from discrete profiles of tracer concentrations and infer the turbulent characteristics.

The primary mechanism controlling the vertical transfer of heat, momentum, and material in the OSBL is turbulent mixing. Therefore, a more important parameter in OSBL dynamics is the mixing layer depth (XLD, denoted by h_ϵ) where turbulent mixing is currently active. Although this may appear to be a minor distinction, as the homogeneous density distribution within the OSBL is a direct result of high levels of turbulent mixing, it is important in order to relate the response of the OSBL to surface forcing. A recent review on mixing layer depths by *Franks* [2014] in relation with Sverdrup's critical depth hypothesis for the North Atlantic phytoplankton bloom [*Sverdrup*, 1953] states that this hypothesis has yet to be thoroughly tested using the XLD and that the distinction between the XLD and the MLD in this case is very important. Currently, there does not exist a robust method to operationally determine the XLD using observations of turbulent quantities, such as dissipation rate of turbulent kinetic energy, ϵ, [*Franks*, 2014].

Many of the parameterizations on energy dissipation and turbulence in the OSBL are based on the assumption that MLD = XLD, which is often not the case in a dynamic ocean [*Brainerd and Gregg*, 1995; *Croot et al.*, 2007; *Cisewski et al.*, 2008; *Noh and Lee*, 2008; *Stevens et al.*, 2011; *Sutherland et al.*, 2014; *Franks*, 2014].

Observations of differences between the MLD and the XLD have been commented on in early microstructure experiments [*Shay and Gregg*, 1986; *Dewey and Moum*, 1990]; however, there have been relatively few studies that have investigated the nature of this difference as it requires specialized instruments to measure turbulent properties and large data sets to quantitatively compare the MLD and XLD.

One of the first studies to look at the difference was that by *Brainerd and Gregg* [1995] using microstructure profiles from the subtropical Pacific. The XLD was defined using both direct measurements of ϵ and Thorpe scales, L_T [*Thorpe*, 1977], in the OSBL. They suggest that Thorpe scales determined from high-resolution temperature profiles gave the best estimates of the XLD during convection when the upper ocean is statically unstable, but with no observations in the upper 10 m they were unable to calculate the XLD during restratification and focused their analysis on profiles during the night. Determining the XLD using ϵ was generally consistent with using L_T although more variable. The calculated XLD by *Brainerd and Gregg* [1995] coincided with density differences from the surface ranging from 0.005 to 0.5 kg m^{-3} with no consensus for an ideal choice for the threshold.

More recently, there have been studies which investigated the MLD and XLD at higher latitudes. During a transect across the north Atlantic at approximately 52°N, *Lozovatsky et al.* [2006] defined the MLD using a density threshold of $\Delta\rho = 0.02\sigma_\theta$, where σ_θ is the surface potential density and the XLD based on ϵ falling to a background dissipation rate of $\epsilon_b = 10^{-8}$ m^2 s^{-3}. *Lozovatsky et al.* [2006] found little difference between the MLD and XLD, with their data spanning a transect of 42 stations across the North Atlantic with generally two to three profiles per station (although sometimes seven to eight). Given the statistical variability of turbulent process, the small number of profiles per station makes it difficult to quantitatively compare the MLD and XLD.

In the subarctic around Svalbard under open-ocean and ice-covered conditions, *Fer and Sundfjord* [2007] defined the MLD using the split-merge method of *Thomson and Fine* [2003] and a XLD using $\epsilon_b = 3 \times 10^{-8}$ m^2 s^{-3}. They found MLD > XLD for the majority of their profiles. They calculated the cross correlation of surface forcing, i.e., wind stress and buoyancy flux, with both the XLD and MLD and found higher correlation coefficients with the XLD. However, turbulence sampling frequency consisted of three profiles every 3–6 h over a station duration of 26–45 h for a total of 81 profiles with 23 of these in ice-covered conditions. Such sparse sampling, especially when they are split up into two different regimes of ice free and ice covered, makes it difficult to quantitatively discuss differences between the MLD and XLD.

In the proximity of an Antarctic Polar Front, *Cisewski et al.* [2008], using a density threshold of 0.02 kg m^{-3} to define the MLD and the same definition for the XLD as *Lozovatsky et al.* [2006], found XLD $\ll$ MLD. This study consisted of a total of 167 microstructure profiles across 33 stations during February and March 2004. Comparisons with the boundary layer depth calculated using a K-profile paramaterization (KPP) model [*Large et al.*, 1994] were improved using the XLD but were still poor during periods of restratification.

Using an ocean general circulation model (OGCM), *Noh and Lee* [2008] directly compared values of the MLD and XLD on a global scale. Two different density thresholds were tested, 0.1 and 0.02 kg m^{-3}, to determine the MLD from the OGCM. The XLD was determined by a decrease in the vertical eddy diffusivity K_ρ to a background value of 10^{-5} m^2 s^{-1} for the first time. It was found that XLD > MLD in regions where strong subsurface shear is present, such as the equatorial ocean and western boundary current regions, and XLD < MLD during early restratification and at high latitudes during convective cooling. In addition, a latitude-dependent $\Delta\rho$ was calculated as the density threshold required to minimize the difference between the OGCM results and climatological data [*Locarnini et al.*, 2006; *Antonov et al.*, 2006]. This dependence has a peak of about 0.09 kg m^{-3} near the equator decreasing to values around 0.02 and 0.03 kg m^{-3} at higher latitudes.

We present observations which explore the phenomenology of the MLD and XLD in the subtropical Atlantic during late summer to obtain a more quantitative view of some of the differences between the MLD and XLD. These observations span the entire mixed layer to the water surface and equally sample all times of the diurnal cycle. An overview of the conditions and observations can be found in section 2. Section 3 investigates the diurnal structure of the MLD and XLD and whether the XLD can be related to the density field. A summary of the results can be found in section 4.

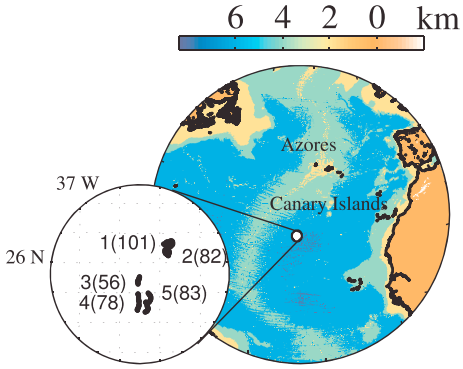

Figure 1. ASIP location for the five deployments during the STRASSE experiment. The number of profiles at each deployment is shown in parenthesis. All deployments are within a radius of 1°. The grid lines on inset map denote 20′ intervals.

2. Observations

Observations were obtained during the SubTRopical Atlantic Surface Salinity Experiment (STRASSE) aboard the N/O *Thalassa*. The site location is shown in Figure 1. This experiment took place during August and September 2012 as part of the larger Salinity Processes in the Upper Ocean Regional Study (SPURS) project. Radiation fluxes and wind speed measurements were recorded aboard the N/O *Thalassa* with the wind stress and buoyancy flux calculated using the TOGA COARE 3.0 algorithm [*Fairall et al.*, 2003].

Figure 2a shows the wind speed U_{10} and surface buoyancy flux B_0 recorded over the five deployments of the Air-Sea Interaction Profiler during STRASSE. The sign convention for B_0 is negative (positive) when the surface buoyancy flux is into (out of) the ocean, i.e., during restratification the surface water becomes more buoyant (i.e., less dense). The buoyancy flux has a typical diurnal pattern of heating due to shortwave radiation during the day followed by cooling at the surface during the night. The wind speeds range from weak to moderate spanning 2 to 10 m s^{-1} and are predominantly northeasterly except during deployment four where they begin shifting to southeasterly in the night.

To accurately determine the buoyancy flux from shortwave insolation into the mixed layer one must account for absorption profile in the water column. Here we follow *Large et al.* [1994] and define $B_f(z)$ as the buoyancy flux to a layer of depth z as

$$B_f(z) = B_0^t + [B_R(0) - B_R(z)] \tag{1}$$

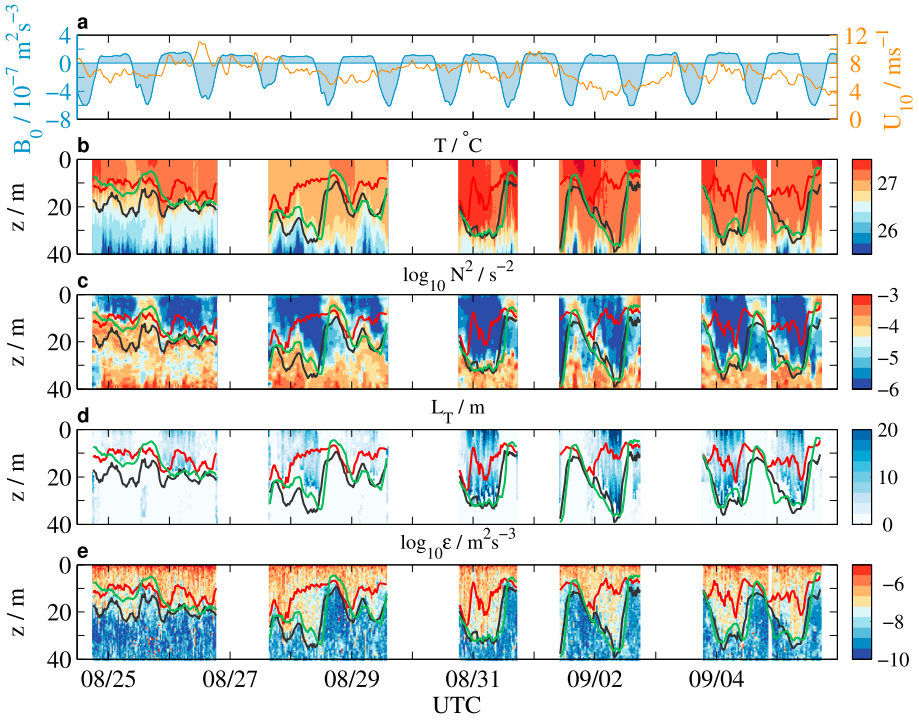

Figure 2. (a) Wind speed (solid orange line) measured at 10 m and surface buoyancy flux (blue region), (b) ocean temperature T, (c) $\log_{10}$ of the buoyancy frequency squared N^2, (d) Thorpe scale L_T, and (e) $\log_{10}$ of the turbulent dissipation rate ϵ. The green, black, and red lines in Figures 2b-2e denote h_ρ, $h_{\epsilon 1}$, and $h_{\epsilon 2}$, respectively.

where B_0^t is the turbulent (i.e., nonradiative) components of the surface buoyancy flux and $B_R(z)$ is the radiation component that decreases with depth. Assuming a simple double exponential profile for the shortwave radiation [*Paulson and Simpson*, 1977], i.e.,

$$B_R(z) = B_R(0)\left[Re^{z/\xi_1} + (1-R)\,e^{z/\xi_2}\right] \tag{2}$$

where z is positive upward, $R = 0.62$, $\xi_1 = 1.5$ m, and $\xi_2 = 20$ m. The values for R, ξ_1 and ξ_2 are for Jerlov type 1A and consistent with clear ocean water similar to what was encountered in this region [*Paulson and Simpson*, 1977]. For a value of $h_\rho = 5$ m, the buoyancy flux correction is $1 - B_R(h_\rho)/B_R(0) = 0.7$. The Monin-Obukhov length L is calculated using (1) as

$$L = -\frac{u_*^3}{\kappa B_f} \tag{3}$$

where $\kappa = 0.4$ is von Kármán's constant and u_* is the friction velocity in water calculated from the wind speed using the TOGA COARE flux algorithm [*Fairall et al.*, 2003]. Here B_f is evaluated at h_ρ as this is expected to be the depth at which buoyancy forces during restratification are expected to extend to, but the use of the MLD or the XLD will have little affect on this parameter as the difference in shortwave radiation between the two depths is small. Henceforth in the manuscript, B_f will denote $B_f(h_\rho)$.

Ocean measurements of the turbulent dissipation rate, temperature, and salinity were obtained with the Air-Sea Interaction Profiler (ASIP), an autonomous microstructure profiler which rises through the OSBL and is specifically designed to measure turbulence properties (for further details, see *Sutherland et al.* [2013], *Ward et al.* [2014]). Presented are 400 profiles made over five deployments during 12 days in late August/early September 2012. The location and number of profiles for the five deployments are shown in Figure 1. The time-depth evolution of temperature T and buoyancy frequency N^2 can be found in Figures 2b and 2c, respectively. The density ratio is given by

$$R_\rho = \frac{\alpha T_z}{\beta S_z}, \tag{4}$$

where α and β are the thermal expansion and the saline contraction coefficients respectively, and T_z and S_z are the vertical gradients of temperature and salinity. Values for R_ρ are typically greater than 2 indicative of temperature-controlled stratification.

The dissipation rate of turbulent kinetic energy, ϵ, is calculated using $\epsilon = 7.5\nu\left\langle u_z^2\right\rangle$, where ν is the kinematic viscosity and u_z is the turbulent vertical shear. Values for ϵ are obtained from 1 s segments of the microstructure shear time series, corresponding to a vertical resolution of about 0.5 m, and averaged over three successive profiles to obtain mean values approximately every hour. Figure 2e shows the measured turbulent dissipation rate for the five deployments.

The MLD, h_ρ, is calculated using a density threshold criterion of 0.03 kg m^{-3} relative to the density at $z_r = 2.5$ m depth. There are several criteria for defining the MLD, but for this study the commonly accepted density threshold suggested by *de Boyer Montégut et al.* [2004] is used and instead the analysis focuses on the XLD [*Brainerd and Gregg*, 1995]. The XLD, h_ϵ, is defined as the shallowest depth where ϵ falls to a certain background level. Profiles of ϵ are also smoothed vertically using a running mean with a half width of 0.5 m to minimize the effect of spatial intermittency giving false positives for the XLD.

Two different background dissipation levels are analyzed to determine the XLD: $\epsilon_{b1} = 10^{-9}$ and $\epsilon_{b2} = 10^{-8}$ m^2 s^{-3}. The XLD determined via each method is designated as $h_{\epsilon 1}$ and $h_{\epsilon 2}$, respectively. The first threshold of 10^{-9} m^2 s^{-3} is determined after inspecting hundreds of profiles and is consistent with XLD definitions from previous studies [*Dewey and Moum*, 1990; *Brainerd and Gregg*, 1995; *Sutherland et al.*, 2014]. However, other studies [*Lozovatsky et al.*, 2006; *Cisewski et al.*, 2008] defined the lower bound of the XLD where ϵ decreased from 10^{-7} to 10^{-8} m^2 s^{-3} so this dissipation threshold is also included. The time series of the MLD and XLD can be found in Figures 2b–2d.

Thorpe scales are calculated as the RMS difference of the reordered temperature profiles [*Thorpe*, 1977] and smoothed using a running mean filter with a half width of 0.5 m. The magnitude of the temperature anomalies were not large enough to use the robust methodology of *Galbraith and Kelley* [1996] and are presented here as a qualitative picture of the XLD analogous to previous studies [*Brainerd and Gregg*, 1995; *Cisewski*

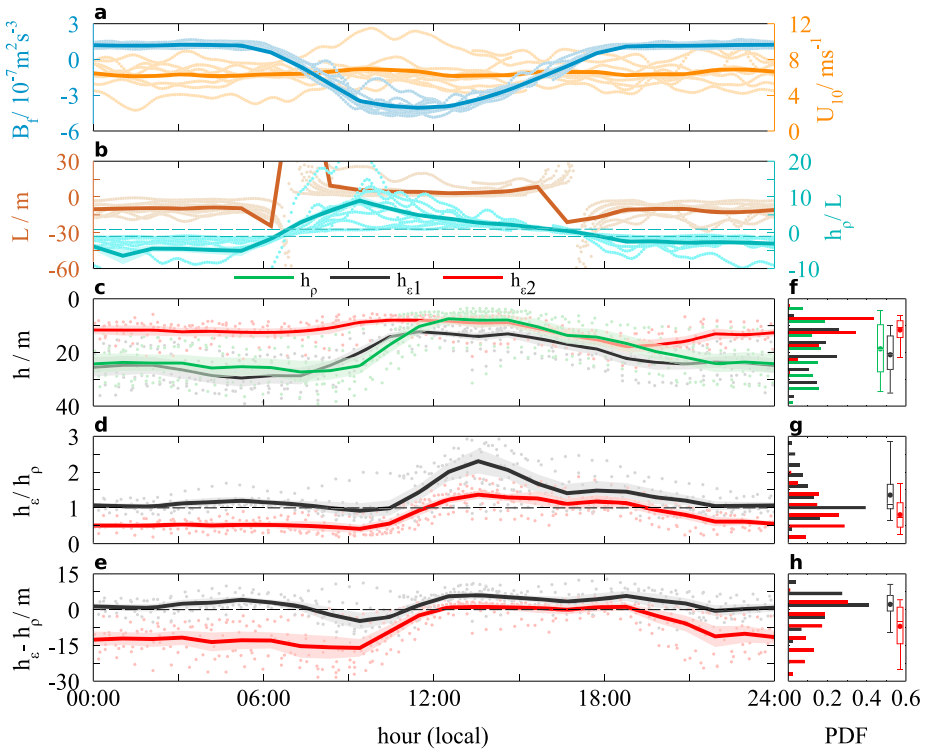

Figure 3. Observations and diurnal phase averages of (a) B_f (blue) and U_{10} (orange), (b) L (brown) and the ratio h_ρ/L (blue-green), (c) mixed h_ρ (green) and mixing layer depths $h_{\epsilon 1}$ (black) and $h_{\epsilon 2}$ (red), respectively), (d) the ratio of the MLD to the XLD, and (e) the absolute difference between the MLD and XLD for the two XLD definitions. The black dashed lines in Figures 3d and 3e denote $h_\epsilon = h_\rho$. (f–h) The histograms for the observations in Figures 3c–3e with the box plots showing the stats for the entire record.

et al., 2008]. Figure 2d shows the measured values of L_T over the ASIP deployments. During convection L_T shows that overturns compare well with h_ρ and $h_{\epsilon 1}$. However, there are no overturns observed during restratification where dissipation rates are high suggesting that L_T is not an ideal proxy for XLD during this time.

3. Results and Discussion

To investigate the diurnal structure of the MLD and XLD, the five deployments are phase averaged as a function of the local time of day to create a single composite day. Phase-averaged values for B_f and U_{10} can be found in Figure 3a. The mean wind speed shows no discernible daily pattern, while the buoyancy flux demonstrates a predictable pattern with the asymmetric shape around noon being due to the greater absorption of shortwave radiation by the deeper MLD in the morning than in the afternoon.

The ratio of h_ρ/L in Figure 3b is often used as a stability parameter for turbulence in the OSBL. During convection, when L is negative, values for h_ρ/L can be $\ll -1$ [*Shay and Gregg*, 1986; *Lombardo and Gregg*, 1989]. However, during restratification $L > 0$ and it is commonly assumed that $h_\rho \leq L$ since buoyancy forces should suppress turbulence at depths greater than the MLD [*Large et al.*, 1994]. However, during the day it was consistently observed that $h_\rho \geq L$ with mean values of h_ρ/L as high as 10 (Figure 3b) during early restratification. Likely possibilities for this could be due to the MLD being less than $z_r = 2.5$ m, or surface gravity waves [*Craig and Banner*, 1994; *Janssen*, 2012] being an extra source of turbulence which is not accounted for in similarity theory, or there is an additional source of kinetic energy not linked to the wind stress such as the diurnal jet described by *Price et al.* [1986]. Since the wind stress is expected to depend on the XLD and the restratification on the MLD, it might be that turbulence and the stabilizing buoyancy flux are far from equilibrium during the day, as noted in the difference between XLD and MLD.

Observations of the phase-averaged values for h_ρ, $h_{\epsilon 1}$ and to a lesser extent $h_{\epsilon 2}$ (Figure 3c) follow a typical diurnal pattern of formation during the late morning followed by a gradual deepening during convection

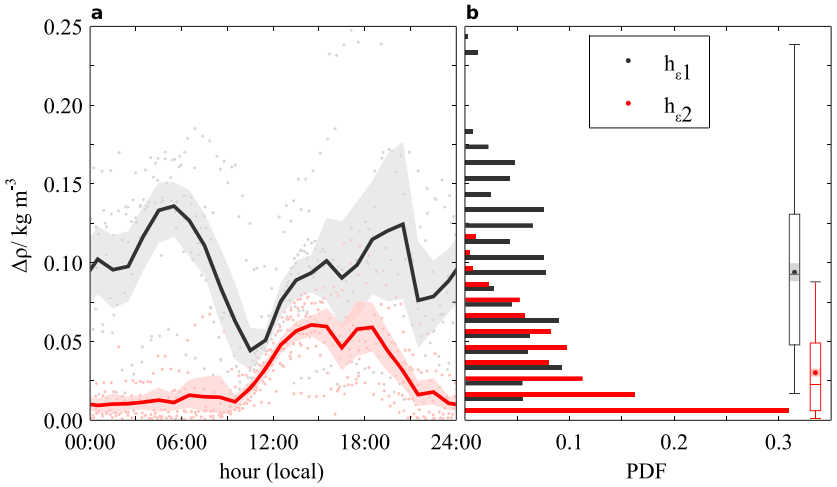

Figure 4. (a) Density difference from the reference level to $h_{\epsilon 1}$ (black) and $h_{\epsilon 2}$ (red) along with the diurnally phase averaged mean and 95% confidence intervals. (b) The histogram of $\Delta\rho$ over the entire period using 0.01 kg m^{-3} bins. The box plots in Figure 4b are for the entire record with the box and whiskers showing the 50th and 95th percentiles, respectively.

[*Lombardo and Gregg*, 1989; *Brainerd and Gregg*, 1995]. In general, h_ρ is a good proxy for $h_{\epsilon 1}$ with the exception of the afternoon as h_ρ underestimates $h_{\epsilon 1}$ by a factor of 1.5–2 suggesting higher dissipation rates at the MLD (see Figures 3d and 3e).

To investigate whether the XLD can be represented by a density threshold we calculate the density difference at the XLD relative to the reference depth $z_r = 2.5$ m, i.e., $\Delta\rho^{\epsilon 1,2} = \rho(h_{\epsilon 1,2}) - \rho(z_r)$, as shown in Figure 4. From 21:00 to 06:00 when $h_\rho \sim h_{\epsilon 1}$, there is a steady increase in $\Delta\rho^{\epsilon 1}$ from 0.08 kg m^{-3} to 0.14 kg m^{-3}. Since $\rho(z_r)$ changes little during this time, the density difference must come from the entrainment of denser water from below the MLD. There is no noticeable pattern with $\Delta\rho^{\epsilon 2}$ as $h_{\epsilon 2}$ does not extend deep enough to encounter any density gradients. This is shown in Figure 4b where $\Delta\rho^{\epsilon 2} < 0.01$ kg m^{-3} when the surface buoyancy flux is positive.

For $\Delta\rho^{\epsilon 1}$ this increasing trend reverses in the morning starting at 06:00 local mean time (LMT) when the sign of B_0 changes, while $\Delta\rho^{\epsilon 2}$ is still predominantly less than 0.01 kg m^{-3}. Beginning around 10:00, both $\Delta\rho^{\epsilon 1}$ and $\Delta\rho^{\epsilon 2}$ steadily increase to values of approximately 0.10 and 0.06 kg m^{-3} in the early afternoon, respectively. This daytime value is maintained, within the confidence intervals, until sunset at around 18:00 LMT where there is a decrease in both $\Delta\rho$ terms.

The buoyancy flux becomes destabilizing at 18:00 LMT where there exists a regime which lasts from this time until 21:00 LMT where $h_{\epsilon 1}$ and $h_{\epsilon 2}$ diverge and head toward their mean depths during convection. This appears to be a transitional period where ϵ at h_ρ is decreasing from 10^{-8} m^2 s^{-3} to 10^{-9} m^2 s^{-3}. After 21:00 LMT $\Delta\rho^{\epsilon 2} \rightarrow 0$ as the convective regime dominates and $\Delta\rho^{\epsilon 1}$ slowly increases due to entrainment as mentioned previously.

The statistics of $\Delta\rho^{\epsilon 1,2}$ over the entire record are shown in Figure 4b. Both distributions are far from normal with $\Delta\rho^{\epsilon 1}$ appearing bimodal between convection and restratification regimes and $\Delta\rho^{\epsilon 2}$ only having the single peak during restratification. The mean values for all observations of $\Delta\rho^{\epsilon 1}$ and $\Delta\rho^{\epsilon 2}$ are 0.09 ± 0.02 and 0.03 ± 0.01 kg m^{-3}. It is interesting to note that the mean value for $\Delta\rho^{\epsilon 1}$ is similar to the mean value of 0.07 kg m^{-3} calculated by *Noh and Lee* [2008] for this latitude, while $h_\rho \sim h_{\epsilon 1}$ during most of the deployments. This is in contrast to the mean value for $\Delta\rho^{\epsilon 2}$, which is equal to the MLD criterion of 0.03 kg m^{-3} even though $h_\rho > h_{\epsilon 2}$ on average and 30% of the $\Delta\rho^{\epsilon 2}$ values being < 0.01 kg m^{-3}.

4. Conclusions

This study represents an investigation of observations of the mixed layer depth (MLD) and mixing layer depth (XLD) under strong diurnal restratification conditions in the subtropical Atlantic during late summer 2012. Presented are 400 microstructure profiles obtained with the Air-Sea Interaction Profiler taken over five

deployments spanning 12 days. The conditions were fairly calm to moderate ($2 < U_{10} < 10$ m s^{-1}) under strong solar heating (1000 W m^{-2}) over the deployments.

To investigate the sensitivity of the XLD definition, two thresholds for the background dissipation rate, $\epsilon_{b1} = 10^{-9}$ and $\epsilon_{b2} = 10^{-8}$ m^2 s^{-3} , were tested. Diurnal variations were observed in both the MLD and XLD which were consistent over all of the deployments with $h_{\epsilon 1} > h_{\epsilon 2} > h_\rho$ during restratification and $h_\rho \sim h_{\epsilon 1} > h_{\epsilon 2}$ during convection. In addition, Thorpe scales L_T were also used to estimate the XLD. While the base of the L_T layer agrees well with h_ρ and $h_{\epsilon 1}$ during periods of positive B_0 (i.e., nighttime convection), L_T fails to represent the daytime evolution of the OSBL when B_0 is negative.

A composite day is created by phase averaging the MLD and XLD by local hour of the day. During convection $h_\rho \sim h_{\epsilon 1}$, while during restratification $h_\rho \sim h_{\epsilon 2}$ which suggests a background dissipation of $\epsilon_{b2} = 10^{-8}$ m^2 s^{-3} in this remnant layer. Larger turbulent dissipation rates are observed during restratification which are not consistent with the stabilizing effect of the buoyancy forcing. Observed values of h_ρ/L are greater than unity during the day suggesting L to be a poor proxy for the MLD during this time. This ratio is even greater if h_ϵ is used instead as $h_\rho < h_{\epsilon 2} < h_{\epsilon 1}$ during this period.

The XLD is presented as a function of the density gradient for the two thresholds for the background dissipation rate. Although $h_\rho \sim h_{\epsilon 1}$, the density difference at $h_{\epsilon 1}$, i.e., $\Delta\rho^{\epsilon 1} = \rho(h_{\epsilon 1}) - \rho(z_r)$ had a mean value 3 times the density threshold of 0.03 kg m^{-3} with two peaks in the distribution of $\Delta\rho$ at the convective maximum and restratification maximum respectively. The mean value for $\Delta\rho^{\epsilon 1}$ is much greater than the accepted range of the density threshold for individual profiles of $0.01 < \Delta\rho < 0.03$ kg m^{-3} [*de Boyer Montégut et al.*, 2004], yet is consistent with a meridionally variable $\Delta\rho$ as shown by *Noh and Lee* [2008].

While it is not surprising that the XLD should be a function of the surface forcing, which will vary regionally and temporally, it is also clear that it will also depend on the MLD and local hydrography. There is a need for more observations of the entire OSBL across different regions and seasons for improved understanding of the associated turbulent processes and provide a sound basis for a better, dynamically motivated, parameterization of the XLD.

Acknowledgments

The authors are grateful for funding support from the National Science and Engineering Research Council of Canada from the scholarship PGSD3-410251-2011, the Office of Naval Research under award N62909-12-1-7064. Support for the cruise was provided by the LEFE/INSU STRASSE/SPURS project, the SMOS project supported by TOSCA/CNES, and the COST Action ES1001. We also extend our gratitude to the Captain and crew of the N/O *Thalassa*. Any requests concerning the data in this paper should be directed to the corresponding author. The authors are grateful to two anonymous reviewers for improving the manuscript.

The Editor thanks two anonymous reviewers for their assistance in evaluating this paper.

References

Antonov, J. I., et al. (2006), *World Ocean Atlas 2005 Volume 2: Salinity,* edited by S. Levitus, NOAA Atlas NESDIS 62 (2), U. S. Government Printing Office, Washington, D. C.

Belcher, S. E., et al. (2012), A global perspective on Langmuir turbulence in the ocean surface boundary layer, *Geophys. Res. Lett.*, *39*, L18605, doi:10.1029/2012GL052932.

Brainerd, K., and M. C. Gregg (1995), Surface mixed and mixing layer depths, *Deep Sea Res.*, *42*(9), 1521–1543.

Castro-Morales, K., and J. Kaiser (2012), Using dissolved oxygen concentrations to determine mixed layer depths in the Bellingshausen Sea, *Ocean Sci.*, *8*(1), 1–10.

Chu, P. C., and C. Fan (2011), Maximum angle method for determining mixed layer depth from Seaglider data, *J. Oceanogr.*, *67*(2), 219–230.

Cisewski, B., V. H. Strass, M. Losch, and H. Prandke (2008), Mixed layer analysis of a mesoscale eddy in the Antarctic Polar Front Zone, *J. Geophys. Res.*, *113*, C05017, doi:10.1029/2007JC004372.

Croot, P., R. Frew, S. Sander, K. Hunter, M. Ellwood, S. Pickmere, E. Abraham, C. Law, M. Smith, and P. Boyd (2007), Physical mixing effects on iron biogeochemical cycling: Fecycle experiment, *J. Geophys. Res.*, *112*, C06015, doi:10.1029/2006JC003748.

de Boyer Montégut, C., G. Madec, A. S. Fischer, A. Lazar, and D. Iudicone (2004), Mixed layer depth over the global ocean: An examination of profile data and a profile-based climatology, *J. Geophys. Res.*, *109*, C12003, doi:10.1029/2006JC004051.

Craig, P. D., and M. L. Banner (1994), Modelling wave-enhanced turbulence in the ocean surface layer, *J. Phys. Oceanogr.*, *24*, 2546–2559.

Dewey, R. K., and J. N. Moum (1990), Enhancement of fronts by vertical mixing, *J. Geophys. Res.*, *95*(C6), 9433–9445.

Fairall, C. W., E. F. Bradley, J. E. Hare, A. A. Grachev, and J. B. Edson (2003), Bulk parameterization of air-sea fluxes: Updates and verification for the COARE algorithm, *J. Clim.*, *16*, 571–591.

Fer, I., and A. Sundfjord (2007), Observations of upper ocean boundary layer dynamics in the marginal ice zone, *J. Geophys. Res.*, *112*, C04012, doi:10.1029/2005JC003428.

Franks, P. J. (2014), Has Sverdrup's critical depth hypothesis been tested? Mixed layers vs. turbulent layers, *ICES J. Mar. Sci.*, 1–11, doi:10.1093/icesjms/fsu175.

Galbraith, P. S., and D. E. Kelley (1996), Identifying overturns in CTD profiles, *J. Atmos. Oceanic Technol.*, *13*, 688–702.

Janssen, P. A. E. M. (2012), Ocean wave effects on the daily cycle in SST, *J. Geophys. Res.*, *117*, C00J32, doi:10.1029/2012JC007943.

Kara, A. B., P. A. Rochford, and H. E. Hurlburt (2000), An optimal method for ocean mixed layer depth, *J. Geophys. Res.*, *105*(C7), 16,803–16,821.

Large, W. G., J. C. McWilliams, and S. C. Doney (1994), Ocean vertical mixing: A review and a model with a nonlocal boundary layer parameterization, *Rev. Geophys.*, *32*(4), 363–403.

Locarnini, R. A., A. V. Mishonov, J. I. Antonov, T. P. Boyer, and H. E. Garcia (2006), *World Ocean Atlas 2005, Volume 1: Temperature*, edited by S. Levitus, 182 pp., NOAA Atlas NESDIS 61 (1), U. S. Gov. Printing Office, Washington, D. C.

Lombardo, C. P., and M. C. Gregg (1989), Similarity scaling of viscous and thermal dissipation in a convecting surface boundary layer, *J. Geophys. Res.*, *94*(C5), 6273–6284.

Lozovatsky, I. D., E. Roget, H. J. S. Fernando, M. Figueroa, and S. Shapovalov (2006), Sheared turbulence in a weakly stratified upper ocean, *Deep Sea Res. Part I*, *53*, 387–407.

Lukas, R., and E. Lindstrom (1991), The mixed layer of the western equatorial Pacific Ocean, *J. Geophys. Res.*, *96*, 3343–3357.
Noh, Y., and W.-S. Lee (2008), Mixed and mixing layer depths simulated by an OGCM, *J. Oceanogr.*, *64*(2), 217–225.
Paulson, C. A., and J. J. Simpson (1977), Irradiance measurements in the upper ocean, *J. Phys. Oceanogr.*, *7*(6), 952–956.
Price, J. F., R. A. Weller, and R. Pinkel (1986), Diurnal cycling: Observations and models of the upper ocean response to diurnal heating, cooling, and wind mixing, *J. Geophys. Res.*, *91*(C7), 8411–8427.
Shay, T. J., and M. C. Gregg (1986), Convectively driven turbulent mixing in the upper ocean, *J. Phys. Oceanogr.*, *16*, 1777–1798.
Stevens, C., B. Ward, C. Law, and M. Walkington (2011), Surface layer mixing during the SAGE ocean fertilization experiment, *Deep Sea Res. Part II*, *58*(6), 776–785.
Sutherland, G., B. Ward, and K. H. Christensen (2013), Wave-turbulence scaling in the ocean mixed layer, *Ocean Sci.*, *9*, 597–608.
Sutherland, G., K. H. Christensen, and B. Ward (2014), Evaluating Langmuir turbulence parameterizations in the ocean surface boundary layer, *J. Geophys. Res. Oceans*, *119*, 1899–1910, doi:10.1002/2013JC009537.
Sverdrup, H. U. (1953), On conditions for the vernal blooming of phytoplankton, *J. Cons.*, *18*(3), 287–295.
Thomson, R. E., and I. V. Fine (2003), Estimating mixed layer depth from oceanic profile data, *J. Phys. Oceanogr.*, *20*, 319–329.
Thorpe, S. A. (1977), Turbulence and mixing in a Scottish loch, *Philos. Trans. R. Soc. London A*, *286*, 125–181.
Ward, B., T. Fristedt, A. H. Callaghan, G. Sutherland, X. Sanchez, J. Vialard, and A. ten Doeschate (2014), The Air-Sea Interaction Profiler (ASIP): An autonomous upwardly-rising profiler for microstructure measurements in the upper ocean, *J. Atmos. Oceanic Technol.*, *31*, 2246–2267, doi:10.1175/JTECH-D-14-00010.1.